Single-cell heterogeneity in interferon induction potential is heritable and governed by variation in cell state

Elizabeth A. Thayer[1], Gabriela Shipman[1], Joel Rivera-Cardona[1], Tarun Mahajan[2,3], Qi Wen Teo[3,4], J. Sebastian Paez[5], Joseph Lederer[3], Jie Chen[6,7,8], Nicholas C. Wu[3,4,7,9], Sergei Maslov[2,3,9,10], Christopher B. Brooke[1,3]*

[1] Department of Microbiology, University of Illinois Urbana-Champaign, Urbana, IL, USA
[2] Department of Bioengineering, University of Illinois Urbana-Champaign, Urbana, IL, USA
[3] Carl R. Woese Institute for Genomic Biology, University of Illinois Urbana-Champaign, Urbana, IL, USA
[4] Department of Biochemistry, University of Illinois Urbana-Champaign, Urbana, IL, USA
[5] Talus Bioscience, Seattle, WA, USA
[6] Department of Cell and Developmental Biology, University of Illinois Urbana-Champaign, Urbana, IL, USA
[7] Department of Biomedical and Translational Sciences, Carle Illinois College of Medicine, University of Illinois Urbana-Champaign, Urbana, Illinois, USA
[8] Cancer Center at Illinois, University of Illinois Urbana-Champaign, Urbana, IL, USA
[9] Center for Biophysics and Quantitative Biology, University of Illinois Urbana-Champaign, Urbana, Illinois, USA
[10] Department of Physics, University of Illinois Urbana-Champaign, Urbana, Illinois, USA
* Corresponding author (cbrooke@illinois.edu)

SUMMARY

Type I and III interferons (IFNs) are among the first lines of defense against viral infection, yet they are generally only produced by a tiny fraction of infected cells. Here, we show that cellular heterogeneity in IFN induction potential upon treatment with immunostimulatory RNA is not due to variability in sensing of stimuli but instead is shaped by heterogeneity in tonic cell signaling state. Using complementary single-cell

approaches, we found that baseline variation in the c-Jun N-terminal kinase (JNK) and activator protein (AP)-1 transcription factor families correlated with *IFNL1* expression predisposition. We further show that drug-based inhibition of JNK signaling virtually eliminates the innate antiviral response to immunostimulatory RNA. Finally, we show that single cell heterogeneity in IFN induction potential is heritable and stably maintained over numerous generations. Together, our study emphasizes the influence of intrinsic variability in cell state on innate immune regulation and IFN induction heterogeneity.

INTRODUCTION

The induction of interferon (IFN) is a critical determinant of infection outcome for a wide variety of viruses[1–5]. Respiratory epithelial cells express both type I and III IFNs (IFNα/β and IFNλ, respectively) as part of their first line of defense against the replication and spread of viruses like influenza A virus (IAV). While most cells in the body can respond to type I IFN, only epithelial cells and a subset of immune cells express the correct receptor for responding to type III IFN[3,6]. Due to this tissue specificity in responsiveness, IFNλ is thought to be less inflammatory while still inducing the expression of IFN-stimulated genes (ISGs) that are important for cellular antiviral defense[1,6].

Retinoic acid-inducible gene I (RIG-I) and melanoma differentiation-associated protein 5 (MDA5) are cytosolic pathogen recognition receptors that recognize viral and synthetic foreign RNAs with distinct molecular features[7–9]. RIG-I and MDA5 share similar downstream signaling pathways, as they activate mitochondrial antiviral-signaling protein (MAVS) and ultimately lead to the nuclear translocation of interferon regulatory factor 3 (IRF3) and the initiation of IFN transcription[6,8]. We and others have demonstrated that only a small percentage of infected cells typically express IFNs, independent of virus type[10–15]. The specific factors contributing to heterogeneity in IFN-induction potential remain poorly understood.

The existence of substantial phenotypic heterogeneity within cellular populations, even for cells of a given “type”, is a well-established phenomenon. Many studies have

investigated how cell-intrinsic factors, such as cell cycle stage, mitogen-activated protein kinase (MAPK) signaling state, and patterns of chromatin accessibility, influence variability in response to a stimulus or other cellular phenotypes[16–21]. Intrinsic 2'-5'-oligoadenylate synthase-like protein (OASL) expression has been recently identified as a critical factor governing cellular heterogeneity in IFN induction potential during IAV infection, but it is not clear whether this effect is IAV-specific[22].

Here, we investigated the sources of cellular heterogeneity in the ability of A549 cells to produce IFN in response to the commonly used RIG-I agonist, polyinosinic:polycytidylic acid (pIC). We used single-cell RNA sequencing and pseudotime analysis to identify transcriptional determinants of IFN induction potential. Additionally, we found that single-cell clonal populations isolated from a single parental population exhibited massive differences in IFN-induction phenotypes that were maintained over numerous generations. This heritable phenotypic variation correlated in part with basal transcriptional and epigenetic profiles. Using multiple approaches, we identified cellular variation in (a) basal expression of ISGs, and (b) MAPK-activator protein (AP)-1 signaling activity as key predictors of the ability of individual cells to mount a robust innate immune response to foreign RNA.

RESULTS

83 **Following pIC treatment, most cells exhibit IRF3 nuclear translocation but do not**
84 **transcribe IFNλ**

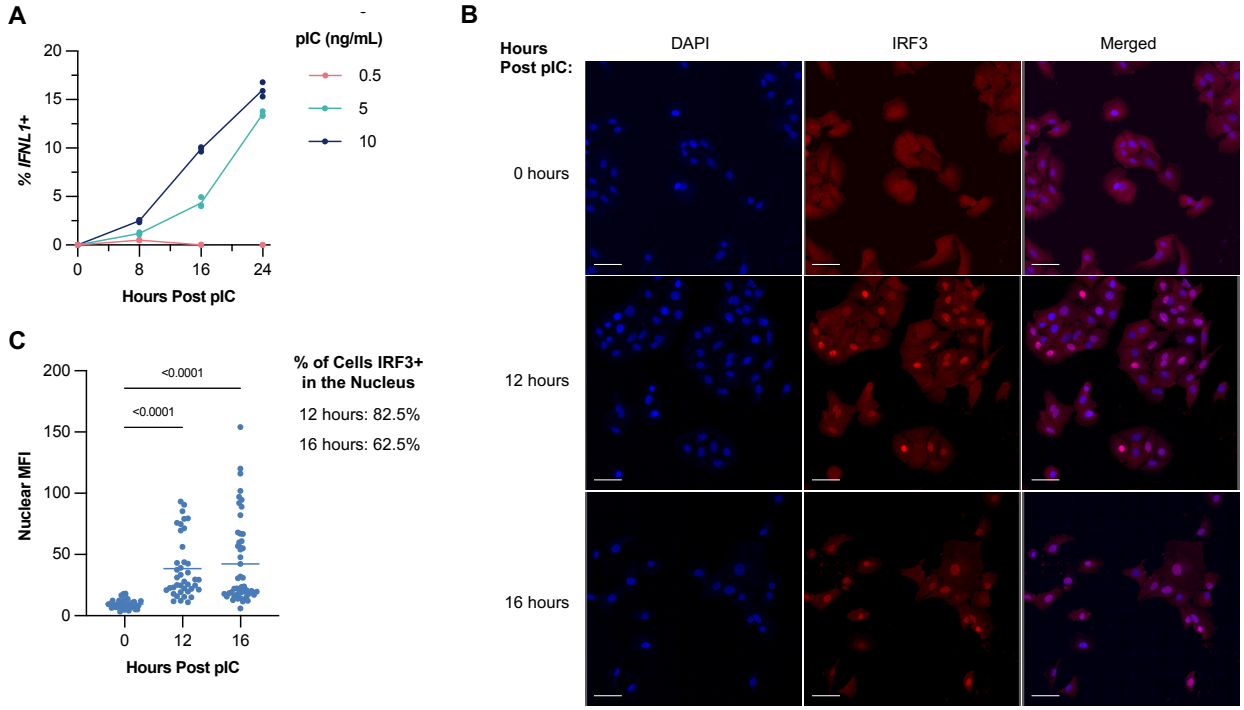

85

86 ***Figure 1. IFNL1 is rarely expressed in A549 cells after pIC stimulation. (A)*** *Percent*
87 *of cells positive for IFNL1 transcripts at 0-, 8-, 16-, and 24-hours post-pIC treatment with*
88 *0.5, 5, and 10 ng/mL concentrations.* ***(B)*** *Representative images of A549 cells*
89 *stimulated with pIC with the nucleus and IRF3 stained. White bars indicate 50 µm.*
90 *Brightness enhanced evenly for publication.* ***(C)*** *Quantification of raw fluorescence of*
91 *IRF3 in the nucleus using Imaris. Significance calculated using Dunnett's multiple*
92 *comparisons. Percent of cells IRF3+ in the nucleus determined by the number of cells in*
93 *the stimulated populations with a higher MFI than the highest untreated cell.*

94

95 Despite the critical importance of the IFN response for host defense, we and others
96 have demonstrated that only a small fraction of cells are generally capable of
97 expressing IFN following viral infection[10–13,23–25]. Viral infection dynamics are highly
98 heterogeneous at the single-cell level, and it is unclear how much of the observed
99 variation in IFN induction is due to cellular heterogeneity in viral processes[14,26,27].

100

101 To examine single-cell heterogeneity in IFN induction without the confounding effects of
102 viral heterogeneity, we treated the human lung adenocarcinoma cell line A549 with
103 increasing concentrations of pIC and quantified *IFNL1* transcription within single cells
104 using hybridization chain reaction[28] fluorescence *in situ* hybridization coupled with flow
105 cytometry (HCR-Flow)[29]. Even after 24 hours post-treatment with the highest dose
106 tested, fewer than 20% of cells expressed detectable levels of *IFNL1* (**Fig. 1A**). Thus,
107 most cells are incapable of expressing IFN in response to pIC, regardless of dosage or
108 timing.
109
110 Activation of pattern recognition receptors like RIG-I or toll-like receptor 3 (TLR3)
111 typically triggers a signaling cascade that results in the phosphorylation and nuclear
112 translocation of IRF3, the primary transcription factor responsible for driving type I and
113 type III IFN induction[6]. If the low frequency of *IFNL1* induction we observed following
114 pIC stimulation was due to a failure to deliver or detect pIC, then we would expect that
115 IRF3 translocation would occur at similarly low frequencies. We treated A549 cells with
116 pIC and measured the percentage of cells in which IRF3 translocated to the nucleus
117 using confocal fluorescent microscopy. We observed IRF3 nuclear translocation in most
118 pIC-treated cells at 12- and 16-hours post-treatment (**Fig. 1B,C**). These results suggest
119 that the low frequency of *IFNL1* induction cannot simply be explained by defects in
120 sensing of pIC or canonical IRF3 signaling.
121

Gene expression profile prior to treatment is predictive of *IFNL1* induction following pIC treatment

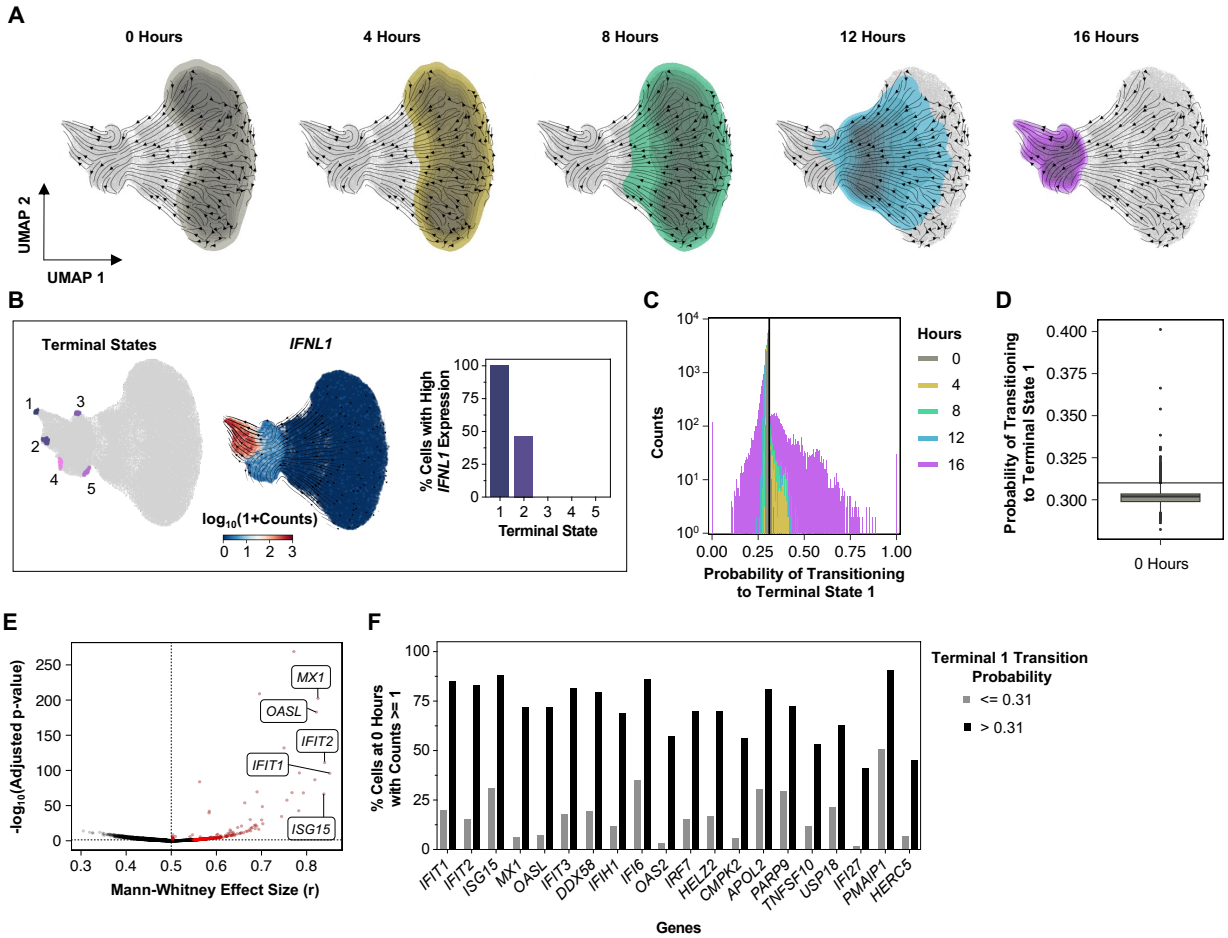

Figure 2. Charting the single-cell transcriptional response to pIC using RNA velocity. (A) *UMAP dimensional reduction of the cells from each time point aggregated together, then colored by time point – time indicating sample collection after 5 ng/mL pIC treatment.* ***(B)*** *UMAP dimensional reduction of all cells from every time point. (Left) Terminal states were calculated using temporal-noSpliceVelo and used to determine the probability that each cell in the dataset would end up in those terminal states. (Middle) UMAP dimensional reduction of all cells colored by* $\log_{10}$*(IFNL1 Counts). (Right) Table showing the percent of cells with IFNL1 counts >= 5 within each terminal state (probability = 1).* ***(C)*** *Distribution of the Terminal 1 transition probability of cells in each collection time point. Line at 0.31 indicating the mean transition probability among the full dataset, ultimately being the threshold for high-probability cells.* ***(D)*** *Distribution of the terminal 1 transition probability per cell in the 0-hour collection time point. Line at*

0.31, the previously established as the threshold for high-probability cells. ***(E)*** *Visualization of the genes significantly more expressed in the high-probability cells at 0 hours. Points in black are the unfiltered genes, and points in red are filtered genes - log_{10}(adjusted p-value) > 1.3 and Mann-Whitney effect size > 0.5.* ***(F)*** *Percent of cells at 0 hours expressing the top 20 genes from the Mann-Whitney analysis, separated by the cells' Terminal 1 transition probabilities.*

Pseudotime analysis has previously been used to identify genes whose baseline expression at the single-cell level correlates with the likelihood that a given cell expresses *IFNL1* in response to IAV infection[22,30]. Since active IRF3 signaling alone is insufficient for robust *IFNL1* expression after pIC stimulation, we sought to use this approach to identify other crucial contributors to the *IFNL1* response following pIC treatment. We isolated A549 cells at 0-, 4-, 8-, 12-, and 16-hours post-pIC treatment for single-cell RNA sequencing (scRNA-seq) to then infer the velocity of individual cells moving through the UMAP dimensions (**Fig. 2A**). This approach identified five terminal states at 16 hours, two of which were *IFNL1*+ (**Fig. 2B**).

We next inferred the probability of each individual cell ending up in terminal state 1, the only terminal state where cells were 100% *IFNL1*+ (**Fig. 2B**). The probabilities are not normally distributed and become increasingly bimodal with time, making a correlation analysis between the probabilities and the gene expression of each cell suboptimal. Instead, we set a threshold for high- and low-probability cells, where "high" is classified as having greater than the mean probability across all time points (**Fig. 2C**). This threshold, when plotted on the 0-hour distribution alone, showed that the high-probability cells were outliers, which was consistent with the rarity of *IFNL1*+ cells (**Fig. 2D**). We used the top 4,000 most variable genes across the time points to conduct a Mann-Whitney test to identify genes that are more likely to be expressed in the high-probability cells at 0 hours than the low-probability cells.

This analysis identified 301 genes expressed at the 0-hour time point with an adjusted p-value lower than 0.05 and an effect size greater than 0.5, indicating they are more

167 likely to be expressed in high-probability cells (**Fig. 2E**). Upon further analysis, we could
168 visualize the result of the test when comparing the percentage of high- or low-probability
169 cells at 0 hours expressing the top 20 genes. All but two of the top genes were
170 expressed in most of the high-probability cells at 0 hours, with all the genes expressed
171 in a greater percentage of high-probability cells (**Fig. 2F**). Additionally, all of the top 20
172 genes have been reported as ISGs, consistent with the emerging idea that intrinsic ISG
173 expression and/or tonic IFN signaling governs IFN induction potential[22,31].
174

175 **Single-cell clones exhibit substantial heritable variation in IFN induction potential**

176 Our results indicated that pre-existing heterogeneity within cell populations underlies
177 variability in IFN-induction potential. We next asked whether this variability in IFN-
178 induction potential was transient or if it could be maintained over multiple generations.
179 To distinguish between these possibilities, we sorted single cells from a population of
180 A549 cells and expanded them into 11 individual clonal lines, denoted ET1-ET11.

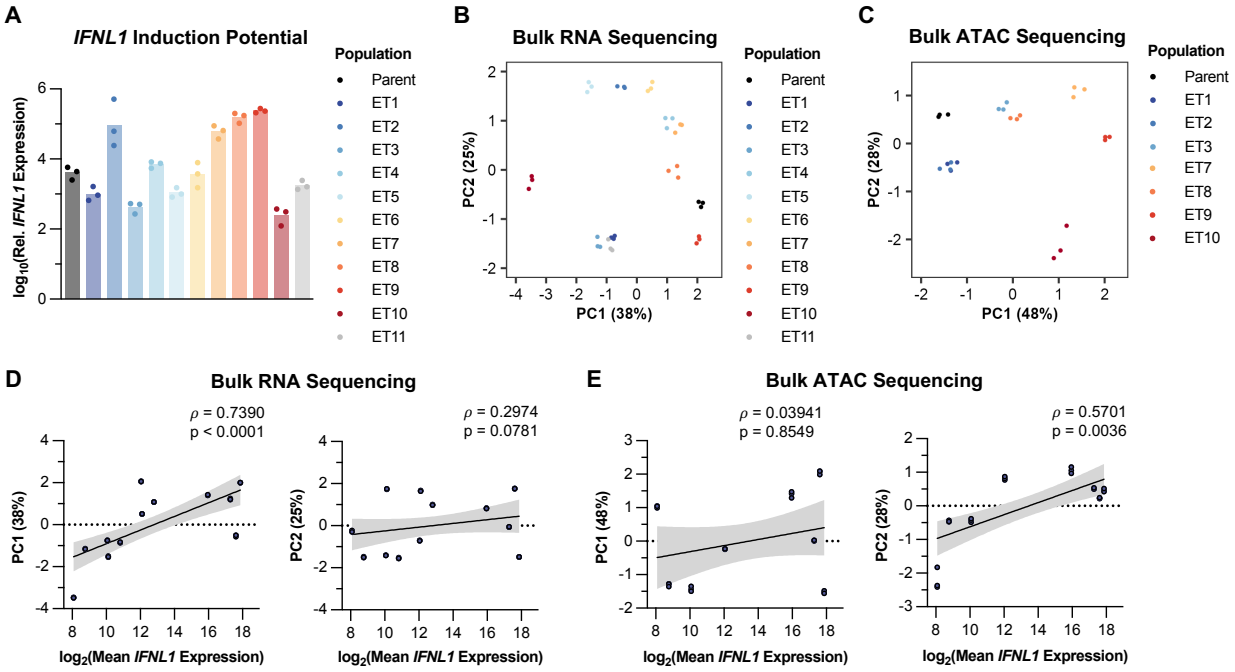

181 ***Figure 3. Sibling clonal cell lines exhibit substantial heritable variability in IFN***
182 ***induction phenotypes. (A)*** *IFNL1 expression 16 hours post 0.5 ng/mL pIC treatment*
183 *among the cell lines was quantified using RT-qPCR. Relative* $\log_{10}$*(ddCt) fold changes*
184 *to their ACTB expression and the mean IFNL1 level from the mock of each respective*
185 *population. One-way ANOVA analysis* $p < 0.0001$*.* ***(B)*** *PCA plot comparing the*

186 *transcriptional profiles of each bulk population.* ***(C)*** *PCA plot comparing the chromatin*
187 *accessibility profiles of each bulk population.* ***(D)*** *Correlation between the PC1 (left) and*
188 *PC2 (right) components of the bulk RNA sequencing data and the* $\log_2$*(Mean IFNL1*
189 *Expression) of each of the clonal lines. Trendline and 95% confidence interval*
190 *generated with simple linear regression.* ρ *and p-value calculated based on Spearman's*
191 *correlation.* ***(E)*** *Correlation between the PC1 (left) and PC2 (right) components of the*
192 *bulk ATAC sequencing data and the* $\log_2$*(Mean IFNL1 Expression) of each of the clonal*
193 *lines. Trendline and 95% confidence interval generated with simple linear regression.* ρ
194 *and p-value calculated based on Spearman's correlation.*
195
196 We treated the parental cell population and the individual clonal lines with 0.5 ng/mL pIC
197 and quantified *IFNL1* induction at 16 hours post-treatment. *IFNL1* transcript levels
198 varied nearly 1000-fold between the individual clonal lines (**Fig. 3A**). Thus, the
199 individual clonal lines exhibited substantial variation in pIC responsiveness that was
200 maintained through the numerous rounds of cell division required to expand them.
201
202 In parallel, we compared the basal transcriptional profiles of the individual clonal lines in
203 the absence of treatment using bulk RNA sequencing and observed that most of the
204 clonal lines diverged substantially from the parental population (**Fig. 3B**). We compared
205 the PC1 component with *IFNL1* induction phenotypes and found a strong correlation
206 between basal transcriptional state and *IFNL1* induction potential (**Fig. 3D**).
207
208 The apparent heritability of heterogeneity in IFN induction phenotypes over numerous
209 generations led us to ask whether this phenotypic variability correlated with any
210 epigenetic signatures. We compared patterns of chromosomal accessibility across the
211 clonal lines using bulk Assay for Transposase-Accessible Chromatin with sequencing
212 (ATAC-seq). We found that global patterns of chromatin accessibility were highly distinct
213 across the clonal lines (**Fig. 3C**). Like what we observed for patterns of transcriptional
214 similarity, ET10 (low *IFNL1* induction) was separated from the group and clearly distinct
215 from ET9 (high *IFNL1* induction). We then asked if variation in the lines' accessibility
216 profiles related to their *IFNL1* responses (**Fig. 3E**). While we did not find a significant

217 correlation between the chromosomal accessibility PC1 and the magnitude of the *IFNL1*
218 response, there was a significant correlation when using the PC2 coordinates (**Fig. 3E**).
219 This suggests that, although the main factor contributing to the heterogeneity in the
220 ATAC data may not be linked to *IFNL1* predisposition, there is significant connection
221 between chromatin accessibility patterns and *IFNL1* expression potential.
222
223 **Variation in basal expression of RIG-I pathway components does not explain the**
224 **heterogeneity in *IFNL1* induction phenotypes**
225 We next sought to determine whether the basal expression patterns of individual
226 transcripts in the clonal populations could also explain heterogeneity in the IFN
227 response to pIC, as we observed in our longitudinal scRNA-seq dataset. We used a
228 generalized linear model, where the x-axis values were the mean $\log_2$ fold changes in
229 *IFNL1* expression of the clonal lines following pIC treatment, and the y-axis values
230 represented the relative expression levels of individual transcripts in the same cell lines
231 in the absence of treatment.
232
233 We first examined the transcripts that encode proteins known to be centrally involved in
234 the RIG-I-based RNA-sensing pathway: *DDX58*, *MAVS*, *TBK1*, and *IRF3*[8,32] (**Fig. 4A,B**).
235 We focused specifically on RIG-I because knocking down other RNA sensors, MDA5
236 (*IFIH1*) and *TLR3*, did not reduce *IFNL1* expression after pIC stimulation as we saw with
237 *DDX58* knockdown, suggesting that the response to pIC in this system is RIG-I-
238 dependent (**Fig. 4A**). While *DDX58, MAVS,* and *TBK1* transcripts did exhibit significant
239 positive correlations with *IFNL1*-induction potential, they only varied in expression levels
240 by 2- to 4-fold across the clonal lines. The expression of the main transcription factor
241 thought to be involved in initiating *IFNL1* expression, *IRF3*, was not significantly
242 correlated with *IFNL1* across the cell lines. Overall, these weak trends appear
243 insufficient to explain the nearly 1000-fold range in IFN expression levels we observed
244 across the clonal lines.

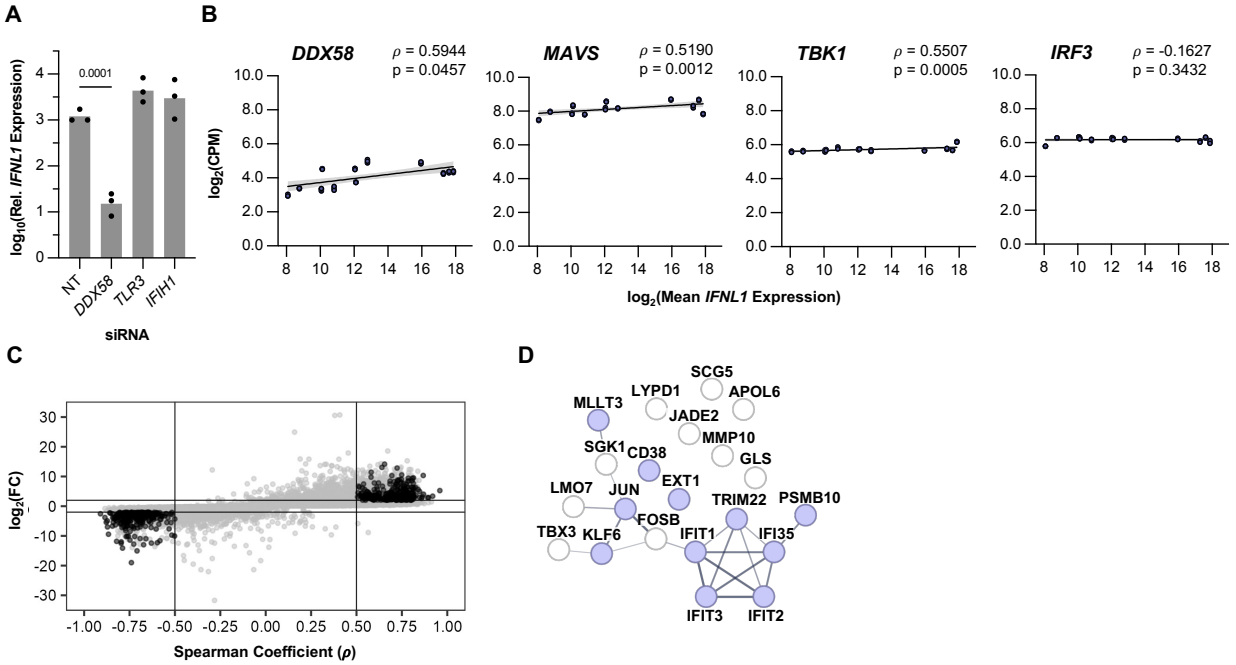

Figure 4. Identification of genes showing a correlation with IFNL1-induction potential. (A) *IFNL1 expression 16 hours post 0.5 ng/mL pIC treatment after 48-hour siRNA treatment was quantified using RT-qPCR. Relative $\log_{10}$(ddCt) fold changes to their ACTB expression and the mean IFNL1 level from the mock of the non-targeting (NT) control. Significance determined by Dunnett's multiple comparisons test.* ***(B)*** *Gene trajectory analysis correlating pIC-induced IFNL1 expression with basal gene expression. Trendline and 95% confidence interval generated with simple linear regression. ρ and p-value generated using Spearman's correlation.* ***(C)*** *Plot of the genes following the generalized linear model (grey), with the genes passing set thresholds of $|\rho| > 0.5$, $-\log_{10}(FDR) > 3$, $|\log_2(FC)| > 2$, and $\log_2(CPM) > 0.1$ (black).* ***(D)*** *STRING analysis of the top genes found in the clonal bulk RNA sequencing and the single-cell data (PPI enrichment $p < 0.0001$). The thickness of the edges indicates the strength of data support for the function and physical protein associations (interaction score > 0.4). Nodes colored purple are annotated to be involved in immune system processes.*

To identify gene products outside of the canonical RIG-I/MAVS pathway that could modulate IFN induction potential, we identified all transcripts that exhibited both (a) a

263 linear trend (|ρ| > 0.5) between expression level and *IFNL1* induction, and (b) a wide
264 range of expression (|$\log_2$FC| > 2) across the clonal lines (**Fig. 4C**). Over 500 genes
265 passed these filtering criteria, so to narrow down the list we examined the common
266 genes present in both the clone and longitudinal scRNAseq datasets. There were 21
267 genes in both lists, with significantly more interactions[33] than expected (PPI enrichment
268 p < 0.0001), suggesting a significant biological connection (**Fig. 4D**). Indeed, there are
269 known ISGs in the list, *TRIM22*, *IFIT1*, *IFIT3*, *IFIT2*, and *IFI35*[34–36], consistent with the
270 observation that basal ISG expression is associated with enhanced IFN induction
271 potential[22,31]. Notably, two components of the AP-1 complex, *JUN* and *FOSB* were also
272 on this list. While cJun is known to bind to the IFNB enhanceosome[37,38], AP-1 signaling
273 has not been implicated in modulating type III IFN expression. These data raised the
274 possibility of AP-1 signaling as another source of heterogeneity in IFN-induction
275 potential.
276
277 **MAPK pathway signaling status modulates *IFNL1* induction potential**

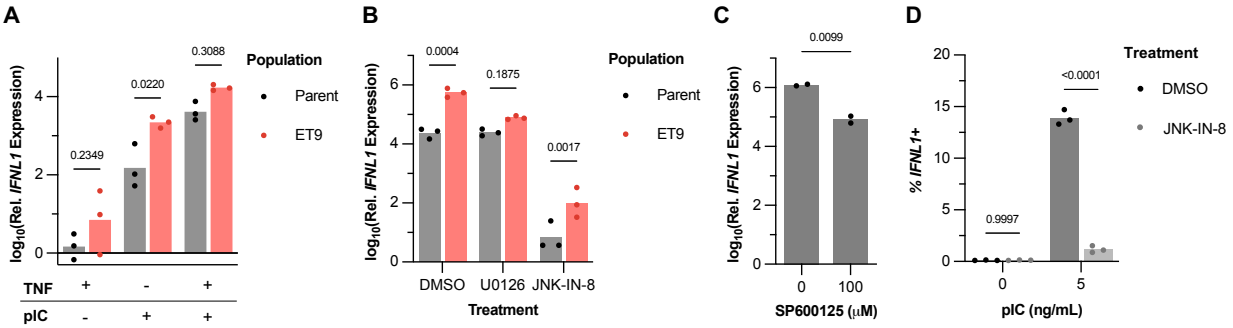

278 ***Figure 5. Investigation of MAPK/JNK signaling status effects on IFN expression.***
279 ***(A)*** *IFNL1 expression of parental and representative "high" IFNL1 expressor A549 clone*
280 *in the presence of 10 μM Ruxolitinib with and without 50 ng/mL TNF pretreatment*
281 *before 0.5 ng/mL pIC treatment for 16 hours. Relative $\log_{10}$(ddCt) fold changes to their*
282 *ACTB expression and the mean IFNL1 level from the mock of each respective*
283 *population. Significance determined by Šídák's multiple comparisons test.* ***(B)*** *IFNL1*
284 *expression in the parental and representative "high" IFNL1 expressor A549 clone was*
285 *assessed following pretreatment with 10 μM U0126 or 24 μM JNK-IN-8, followed by 0.5*
286 *ng/mL pIC treatment for 16 hours. Relative $\log_{10}$(ddCt) fold changes to their ACTB*
287 *expression and the mean IFNL1 level from the mock of each respective population.*

Significance determined by Šídák's multiple comparisons test. ***(C)*** *IFNL1 expression of A549 cells after 100 μM SP600125 treatment and subsequent stimulation with 5 ng/mL pIC for 16 hours. Relative log_{10}(ddCt) fold changes to their ACTB expression and the mean IFNL1 level from DMSO without pIC. Significance determined by an unpaired t-test.* ***(D)*** *HCR-Flow measuring the percentage of cells positive for IFNL1 transcripts after DMSO or 24 μM JNK-IN-8 pre-treatment, then 5 ng/mL pIC stimulation for 16 hours. Significance determined by Šídák's multiple comparisons test.*

AP-1 activity is heavily influenced by upstream MAPK signaling and is potently activated by tumor necrosis factor (TNF)[39–42]. To examine the role of AP-1 activity in IFN induction heterogeneity in our system, we first asked how activation of MAPK signaling via TNF pretreatment affected IFN induction by pIC in both the parental A549 cell population and the ET9 clonal line that exhibited a high IFN induction phenotype. However, we wanted to focus only on TNF's potential role in *IFNL1* induction, so we used ruxolitinib[43] pre-treatment to block the JAK/STAT signaling pathway, which is involved in TNF signaling[44]. We found that treatment with TNF alone elicited very little *IFNL1* expression at similar levels in both parental and ET9 populations, indicating that (a) TNF treatment is insufficient to trigger IFN induction in A549 cells, and (b) that TNF responsiveness does not vary significantly across clonal A549 lines, contrasting with pIC responsiveness. Despite TNF not inducing a large amount of *IFNL1* alone, we observed that TNF pre-treatment synergized with pIC stimulation to drive robust *IFNL1* induction in both cell lines, well beyond what would be expected if the contributions of pIC and TNF were simply additive. Importantly, TNF pretreatment reduced variation in IFN induction between parental and ET9 populations, suggesting that variability in IFN induction between clonal lines can be partially overcome by activating the MAPK signaling network (**Fig. 5A**).

We then aimed to inhibit the two MAPKs known to regulate AP-1, JNK and extracellular signal-regulated kinases (ERK), and to examine how this inhibition affected *IFNL1* expression[45,46]. Inhibition of ERK with the MEK inhibitor U0126 did not have a drastic effect on *IFNL1* expression in either population, although it did eliminate the difference

319 between parent and ET9 (**Fig. 5B**). On the other hand, JNK inhibition with the highly
320 selective JNK inhibitor JNK-IN-8[47] almost completely eliminated *IFNL1* expression in the
321 parent and drastically reduced its expression in ET9 (**Fig. 5B**). We also used another
322 JNK inhibitor, SP600125, to affirm our finding with JNK-IN-8. Although it was less
323 dramatic than with JNK-IN-8 treatment, JNK inhibition using SP600125 did lead to a
324 significant decrease in *IFNL1* expression. (**Fig. 5C**). As a follow-up, we wanted to see if
325 this reduction in expression was from the same number of cells producing less *IFNL1*,
326 or if inhibition of JNK signaling changed the number of cells able to produce *IFNL1* in a
327 population. JNK-IN-8 pre-treatment significantly affected the percentage of cells
328 responsive to pIC stimulation (**Fig. 5D**). Together, these data suggest a role for the
329 MAPK/AP-1 signaling network in governing single-cell heterogeneity in IFN induction
330 potential.
331
332 **JNK-IN-8 treatment largely eliminates the transcriptional response to pIC**
333 Given that IFN induction was obliterated by JNK-IN-8 treatment, we next asked whether
334 the entire global transcriptional response to pIC was JNK-IN-8-sensitive. We stimulated
335 A549 cells with pIC in the presence or absence of JNK-IN-8 and the JAK1/JAK2
336 inhibitor ruxolitinib[43] (to block effects downstream of IFN signaling) and quantified
337 transcriptional changes using bulk RNA-seq 16 hours after pIC treatment. As expected,
338 ruxolitinib treatment partially decreased pIC-stimulated *IFNL1* expression in A549s,
339 likely due to the role of IFN signaling in enhancing IFN induction (**Fig. 6A**).
340
341 Treatment with either pIC, JNK-IN-8, or ruxolitinib alone had profound, divergent effects
342 on the cellular transcriptome (**Fig. 6B**). Interestingly, JNK-IN-8 and ruxolitinib pre-
343 treatment shifted the transcriptional phenotype of pIC-treated cells to closely resemble
344 that of the DMSO-only controls. This suggested that almost the entirety of the
345 transcriptional response to pIC in A549 cells could be eliminated by inhibiting both JNK-
346 and JAK-dependent signaling.
347

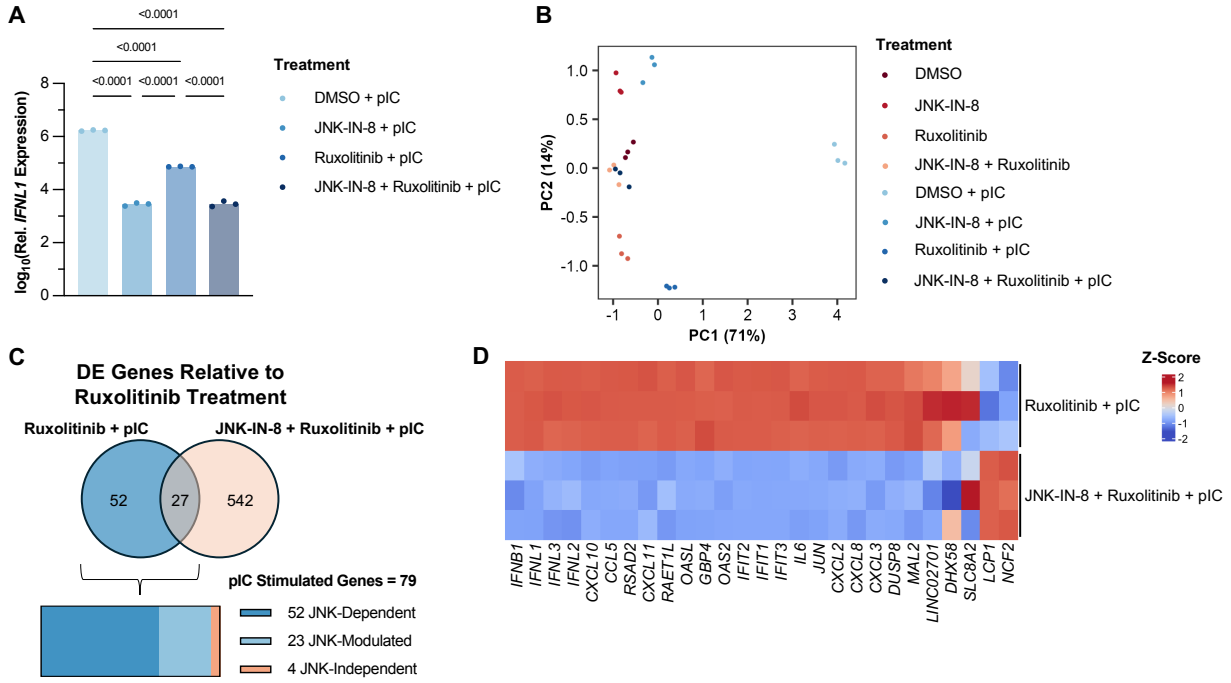

Figure 6. JNK-IN-8 treatment virtually eliminates the innate immune response to pIC. (A) *IFNL1 expression 16 hours post-treatment with 5 ng/mL pIC. Log_{10}(ddCt) relative to ACTB and DMSO-treated control. Inhibitor treatments with 10 μM ruxolitinib and 24 μM JNK-IN-8 4 hours before pIC stimulation. Significance determined by Tukey's multiple comparisons test.* ***(B)*** *PCA plot comparing the transcriptional profiles of the different treatment groups.* ***(C)*** *Venn diagram showing the distinct and shared DE genes in the Ruxolitinib+pIC and JNK-IN-8+Ruxolitinib+pIC treatments. Parts of a whole diagram below detailing what genes of the pIC-stimulated group are JNK-dependent.* ***(D)*** *Heatmap comparing the expression of the shared 27 DE genes of Ruxolitinib+pIC and JNK-IN-8+Ruxolitinib+pIC. Gene expression is relative between the two conditions and is represented by the Z-score.*

To specifically define the JNK-dependent portion of the transcriptional response to pIC, we analyzed the differentially expressed (DE) genes in either the ruxolitinib+pIC or JNK-IN-8+ruxolitinib+pIC group relative to the ruxolitinib-only group (**Fig. 6C**). Fifty-two transcripts were significantly upregulated in the ruxolitinib+pIC group but not in the JNK-IN-8+ruxolitinib+pIC group, likely representing the portion of the transcriptional response to pIC that was fully JNK-dependent. Twenty-seven additional transcripts were DE

366 compared to ruxolitinib-only controls in both groups, but only four appeared unaffected
367 by the presence of JNK-IN-8, suggesting that almost the entirety of the transcriptional
368 response to pIC is fully or partially dependent upon JNK signaling (**Fig. 6D**).
369
370 **DISCUSSION**
371 In this study, we sought to identify the intrinsic sources of cell-to-cell heterogeneity in
372 IFN induction potential observed across a variety of infection systems[10,12–15,22,23,31],
373 using the synthetic dsRNA RIG-I ligand pIC. Using multiple complementary approaches,
374 we identified both basal expression of ISGs and the MAPK/AP-1 signaling network as
375 important determinants of single-cell IFN-induction heterogeneity in this system. While
376 we previously identified a role for intrinsic ISG expression (specifically OASL) in
377 influencing IFN induction potential during IAV infection[22], our data here extend that
378 finding to other stimuli and identify a new role for MAPK/AP-1 signaling in influencing
379 cellular heterogeneity in innate immune function.
380
381 Both our longitudinal scRNAseq experiment and our transcriptional analyses of single-
382 cell-derived clones identified the AP-1 transcription factors *JUN* and *FOSB* as correlates
383 of IFN-induction potential. These factors are activated downstream of the MAPK family,
384 an incredibly complex and highly conserved network of signaling molecules that
385 collectively integrate numerous diverse inputs to regulate multiple aspects of cellular
386 behavior, including innate immune function[48–50]. Because of the large number of input
387 signals that can modulate MAPK activity, including cytokines and various sources of
388 cellular stress, the potential involvement of MAPK/AP-1 signaling opens the door to the
389 possibility of a variety of external and internal stimuli contributing to the tuning of IFN
390 induction potential at the single-cell level.
391
392 To examine the role of the MAPK network and the downstream AP-1 family transcription
393 factors in governing cellular heterogeneity in IFN induction, we took two approaches,
394 each with significant caveats. First, we tried maximizing MAPK signaling activity by
395 pretreating with TNF in the presence of the JAK/STAT inhibitor ruxolitinib. Our findings
396 confirmed previous work demonstrating that TNF can enhance the production of type I

397 IFNs and their downstream ISGs[44,51–53]. Importantly, they also showed that TNF
398 pretreatment reduced the variability in IFN-induction potential between clonal lines of
399 A549 cells. While this is consistent with a role for MAPK signaling in IFN-induction
400 heterogeneity, the effects of TNF stimulation are many (including activation of IRF1[44,52–
401 54]), and thus these results do not provide much clarity on the specific players involved.
402
403 Second, we tried inhibiting AP-1 function by treating with drugs that target the two main
404 pathways connecting MAPK signaling and AP-1: JNK and ERK. Inhibition of JNK
405 activation nearly eliminated bulk expression of *IFNL1* and nearly every other transcript
406 induced by pIC stimulation. JNK-IN-8 treatment also significantly decreased the
407 percentage of cells capable of expressing *IFNL1* after pIC stimulation. In contrast, ERK
408 inhibition had no appreciable effect on IFN induction, suggesting that the effects of
409 MAPK activity on IFN induction are mediated through JNK. While JNK-IN-8 treatment
410 has been reported to exhibit a high degree of specificity for JNK relative to other
411 kinases[45], it is impossible to guarantee specificity at the μM concentrations used here.
412 While we found similar effects on IFN induction with the alternative JNK inhibitor
413 SP600125, we cannot rule out that the effects we observed with JNK inhibitors are due
414 to off-target effects. At a minimum, our results point towards a potential therapeutic role
415 for JNK-IN-8 or other JNK inhibitors in the treatment of some interferonopathies.
416
417 Our finding that cellular heterogeneity in IFN-induction potential could be stably
418 maintained through multiple generations has important implications for understanding
419 innate immune function within epithelial tissues. If there is significant heterogeneity
420 within populations of epithelial stem cells, this heterogeneity could be passed on
421 through transiently amplifying cells into descendant populations of differentiated
422 epithelial cells[55]. This could potentially result in microenvironments with differing
423 sensitivities to innate immune stimuli across the epithelia.
424
425 Though we could not pinpoint a specific mechanism underlying this heritability, it is likely
426 epigenetically encoded. If there were no epigenetic basis for single-cell heterogeneity in
427 pIC responsiveness, we would expect that the numerous generations required to

428 expand individual sorted cells into the clonal lines we examined would eliminate any
429 transient variability in responsiveness seen at the single-cell level. A large body of work
430 has demonstrated that cellular populations can exhibit substantial single-cell
431 heterogeneity in epigenetic states, which gives rise to phenotypic variation[19,21]. These
432 results are also consistent with previous studies demonstrating that IFN expression is
433 subject to epigenetic regulation[20,56–59] and that single cells isolated from populations
434 during CRISPR knockout generation are often not representative of the population as a
435 whole[60,61]. Our results further emphasize the need for extreme caution when interpreting
436 data generated from single-cell clones (*e.g.,* CRISPR knockouts).
437
438 Our results point towards important roles for MAPK/AP-1 signaling and intrinsic ISG
439 expression patterns in determining the fraction of cells capable of responding to viral
440 stimuli by producing IFNs. Because the IFN response is highly non-linear, even small
441 changes in the percentage of IFN-producing cells can have disproportionate effects on
442 the kinetics and magnitude of the downstream antiviral response[62]. The percentage of
443 cells capable of IFN induction effectively sets a threshold of how far viral replication
444 must proceed before triggering an IFN response. Such a system could help avoid
445 unnecessary IFN induction by harmless exposures to PRR ligands, such as might be
446 expected during (a) the limited viral replication that can occur within an immune host, or
447 (b) a transient breakdown in metabolism or containment of host-encoded
448 immunostimulatory RNAs. Future studies should more closely examine how patterns of
449 single-cell heterogeneity in IFN-induction potential vary across different cell populations
450 and environmental contexts.
451
452 **LIMITATIONS OF THE STUDY**
453 There are significant limitations surrounding the use of transformed cell lines like the
454 A549 human lung adenocarcinoma cell line used throughout this study. These cells
455 diverge from primary epithelial cells in many important ways, including genomic stability
456 and immune function. Further work is needed both in primary cell systems and *in vivo* to
457 validate and extend the results we report here. As indicated above, it is impossible to
458 rule out off-target effects when evaluating the results obtained using the JNK inhibitor

drugs. Both our analyses of single-cell clones and our single-cell pseudotime analysis approaches rely upon correlative results, which do not conclude any causal relationship. More work is needed to firmly establish causal relationships.

RESOURCE AVAILABILITY

Lead contact

All additional questions for further information or resources should be directed to the lead contact, Chris Brooke (cbrooke@illinois.edu).

Materials availability

Clonal lines and other reagents are available upon request.

Data and code availability

All sequencing data can be found at NCBI GEO under accession numbers GSE313066, GSE313067, GSE313068, and GSE313071. The code used for the data analysis in this manuscript can be found at https://github.com/BROOKELAB.

ACKNOWLEDGEMENTS

We thank the scientists at the sequencing facility in the Roy J. Carver Biotechnology Center for their help with consultation and preparation for our many sequencing experiments. We also thank those at HPCBio, specifically Drs. Chris Fields and Jenny Drnevich, for their guidance in navigating downstream data processing and analysis for the sequencing experiments. Additionally, Dr. Kevin Van Bortle was a great source of advice with the ATAC sequencing analysis.

C.B.B was supported by NIH R01 AI139246, NIH R01 AI179910. N.C.W. was funded by NIH R01 AI165475. J.C. was supported by NIH R01 GM089771. S.M. was supported by NSF 2107344.

AUTHOR CONTRIBUTIONS

C.B. and E.A.T. conceptualized the study. E.A.T., G.S., J.R.C., and J.L., performed all the experiments. E.A.T. and J.S.P. conducted all of the bulk RNA and ATAC sequencing data processing and analysis. E.A.T. processed the single-cell RNA sequencing data for

T.M. to perform the temporal-noSpliceVelo analysis, and then E.A.T., with help from J.R.C., analyzed the data further. S.M. and T.M. conceptualized temporal-noSpliceVelo. Q.W.T., J.C., and N.C.W. provided critical reagents. E.A.T. and C.B. wrote the manuscript.

DECLARATION OF INTERESTS

The authors declare the following financial interest: J.S.P. is an employee of Talus Biosciences, Inc., a company developing anticancer therapeutics. All other authors declare no competing interests.

MATERIALS AND METHODS

Cells

Human lung epithelial cells (A549) were a gift from Dr. Jonathan Yewdell and maintained in Gibco's Dulbecco's Modified Eagle's Medium (DMEM) high glucose supplemented with GlutaMax and sodium pyruvate, along with the addition of fetal bovine serum (Avantor) for an ending concentration of 8.3%. The cells were cultured at 37°C with 5% CO_2.

Generation of single cell clonal lines

Low-passage A549 cells were collected for FACS and individual cells were distributed into a 96-well flat-bottom plate (Falcon) containing culture media + 5% Penicillin/Streptomycin (Gibco), with 1 cell per well. The wells were then monitored daily until colonies were visible under a microscope. Each well was tracked for whether it contained only one colony or multiple colonies (indicating that the seeding was not perfectly 1 cell per well). Only wells containing a single colony were trypsinized (0.05% Trypsin-EDTA 1X, Gibco) when confluent and expanded into 24-well plates, then into 6-well plates, and finally into T-25 then T-75 flasks. The clones (ET1-11) were numbered based on the order of initial collection.

Polyinosinic:polycytidylic acid (pIC) treatment

520 A549 cells were transfected using Lipofectamine 3000 (Invitrogen) with the synthetic
521 double-stranded RNA, pIC (Poly(I:C) LMW, InvivoGen), for the indicated time points.
522 After the specified treatment times, the samples were collected based on the specific
523 downstream quantification method.
524
525 **siRNA treatment**
526 We used Dharmacon ON-TARGETplus SMARTpool siRNA (Horizon Discovery) to
527 knock down gene transcripts. The siRNAs used were against human DDX58 (Gene ID:
528 23586, L-012511-00-0005), TLR3 (Gene ID: 7098, L-007745-00-0005), IFIH1 (Gene ID:
529 64135, L-013041-00-0005), and non-targeting control (D-001810-10-05). The A549s
530 were transfected with 30 nM siRNA using Lipofectamine RNAiMAX (Invitrogen)
531 according to the manufacturer's protocol. The cells were incubated for 48 hours, then
532 the RNA was extracted to determine knockdown efficiency, or the cells were treated with
533 pIC as previously described.
534
535 **Tumor necrosis factor (TNF) treatment**
536 JAK1/2 inhibition was achieved using ruxolitinib (MedChemExpress), which was first
537 dissolved in DMSO and diluted to 10 μM in cell culture media. The cells were treated
538 with ruxolitinib for 4 hours before TNF, pIC, or both were added to the cells and
539 remained in the media for the entirety of the incubation. Recombinant human TNF
540 (PeproTech) was diluted to 50 ng/mL in culture media, then added to cells 30 minutes
541 before the cells were either collected for western blot analysis or transfected with pIC.
542 The pIC-transfected cells were incubated for 16 hours, after which the RNA was
543 collected for gene expression analysis.
544
545 **Drug treatments**
546 All inhibitors were dissolved in DMSO and stored at -70°C in single-use aliquots for
547 long-term storage. Each inhibitor was diluted to its working concentration, with the
548 DMSO concentration not exceeding 1%, in culture media and remained in the culture
549 media throughout the experiment. The cells were incubated with the inhibitors for 4
550 hours before the addition of their specified stimulus.

551

552 **RNA isolation, reverse transcription, and gene expression quantification**

553 The cells were first washed with 1X DPBS (Gibco), then lysed with Buffer RLT
554 (QIAGEN). The samples were then collected and processed using the RNeasy Mini Kit
555 (QIAGEN) according to the manufacturer's protocol, or frozen at -70°C until further
556 processing could be performed. cDNA synthesis was performed using the Verso cDNA
557 Synthesis Kit (Thermo Scientific) with the provided anchored oligo(dT) primers,
558 according to the user guide. qPCR could then be performed on the QuantiStudio 3
559 system (Applied Biosystems) with TaqMan reagents (Life Technologies). Gene
560 expression levels were calculated using ΔΔCt, normalizing to ACTB.

561

562 **Hybridization chain reaction combined with flow cytometry (HCR-Flow)**

563 HCR-Flow was performed as previously described[29]. As stated, a single cell suspension
564 of A549 cells was prepared by incubating cells with 0.05% Trypsin-EDTA (Gibco) at
565 37°C for 5 minutes. The cell suspension was washed with DPBS (Gibco) and fixed with
566 4% formaldehyde (Thermo Scientific) for 30 minutes at 4°C. After incubation, cells were
567 washed twice with PBST and incubated overnight in 70% ethanol. The single cell
568 suspension was washed twice with DPBS + 0.1% Tween20 (PBST) (Thermo Scientific
569 Chemicals) and incubated with amplification buffer (Molecular Instruments) for 30
570 minutes at 37°C. After incubation, 1 μM of each probe (Molecular Instruments) was
571 added to the cell suspension and incubated overnight at 37°C. Cells were resuspended
572 in probe wash buffer (Molecular Instruments), incubated at 37°C for 10 minutes, and
573 this was repeated three times. Cells were washed once with 5x sodium chloride sodium
574 citrate + 0.1% Tween 20 (SSCT) and incubated in amplification buffer (Molecular
575 Instruments) at RT for 30 mins. After incubation, 3 μM of each snap-cooled hairpin
576 (Molecular Instruments) was added to the cell suspension and incubated at RT
577 overnight. Cells were washed twice with SSCT and analyzed using BD FACSymphony
578 A1.

579

580 **Immunofluorescence microscopy and analysis**

581 A549 cells were transfected with 5 ng/mL pIC and incubated for 16 hours before they
582 were washed with DPBS and fixed with 4% formaldehyde (Thermo Scientific) for 30
583 minutes at 4C. The cells were then washed with PBST three times at RT, permeabilized
584 with DPBS + 0.2% Triton X-100 (Thermo Scientific Chemicals) for 30 minutes, and
585 washed again three times with PBST. Then the cells were blocked with DPBS + 0.1%
586 TritonX-100 + 4% FBS for 30 minutes at RT and incubated with Mouse anti-IRF3
587 (10949S, CST) in the blocking solution for 1 hour at RT. After washing three times with
588 PBST, the cells were incubated with AlexaFluor 647 AffiniPure Donkey anti-Mouse (715-
589 605-150, Jackson ImmunoResearch) in blocking buffer for 1 hour at RT. The cells were
590 washed three times with PBST, stained with DAPI (Thermo Fisher) in PBST buffer for 10
591 minutes at RT, then washed three more times in PBST. Finally, the slides were mounted
592 using ProLong Gold antifade reagent (Invitrogen), and a coverslip was set and sealed
593 with nail polish before imaging on a Zeiss LSM 880.
594
595 The images were analyzed using Imaris (Oxford Instruments). Briefly, DAPI was used to
596 generate 3D objects, and the mean fluorescence intensity (MFI) of the IRF3 signal
597 within the nuclei was recorded. The MFI of untreated versus pIC-treated cells could then
598 be compared to determine the nuclear translocation of IRF3.
599
600 **Bulk RNA sequencing of clonal cell lines**
601 The A549 cell lines ET1-11, along with the parent line, were initially seeded at 1 million
602 cells per well in 6-well plates with three wells per cell line. 24 hours after seeding, the
603 cells were collected, and RNA was isolated as previously described. The Roy J. Carver
604 Biotechnology Center (RJCBC) sequencing facility was responsible for all downstream
605 preparation and sequencing. This included QC, MiSeq (Illumina) titration, cDNA library
606 generation using the TruSeq Stranded mRNAseq Sample Prep kit (Illumina), and
607 sequencing on the NovaSeq 6000 (Illumina) using a S4 flow cell with 2x150nt reads.
608
609 **Bulk RNA sequencing of JNK-IN-8, Ruxolitinib, and pIC-treated A549s**
610 The A549 cells were seeded at 1 million cells per well in 6-well plates, with three wells
611 per condition. Cells were either treated with 1% DMSO, 24 μM JNK-IN-8, 10 μM

612 ruxolitinib, or both inhibitors for 4 hours, then 5 ng/mL pIC was added as previously
613 described. The cells were incubated for 16 hours, then collected for sequencing using
614 the same methods. These samples were also processed and sequenced at the RJCBC
615 sequencing facility. The libraries were prepared with the Kapa Hyper Stranded mRNA
616 library kit (Roche) and sequenced using the NovaSeq X Plus (Illumina) on one 10B lane
617 with 1x100nt reads.
618
619 **Bulk ATAC sequencing of clonal cell lines**
620 The A549 cell lines ET1-11, along with the parent line, were initially seeded at 1 million
621 cells per well in 6-well plates with three wells per cell line. 24 hours after seeding, the
622 cells were trypsinized and collected on ice for transport to the RJCBC for processing.
623 This includes library preparation with the ATACseq kit from Active Motif and sequencing
624 on the NovaSeq X Plus (Illumina) on one 10B lane with 2x150nt reads.
625
626 **Single-cell RNA sequencing of A549s**
627 A549 cells were seeded at 1 million cells per well in 6-well plates. 24 hours after
628 seeding, the cells were treated with 5 ng/mL pIC as previously described. The cells
629 were then collected at their specific time points, transported to the RJCBC on ice, and
630 given to the sequencing facility for further processing and sequencing. The libraries
631 were prepared with the Chromium Next GEM Single Cell Fixed RNA Sample
632 Preparation Kit for Human Transcriptome (10X Genomics) and sequenced using a
633 NovaSeq X Plus (Illumina) on two 10B lanes with 28x150nt reads.
634
635 **Modification and use of temporal-noSpliceVelo for the single-cell RNA**
636 **sequencing dataset**
637 This method of expression-trajectory analysis has been detailed in previous work[22,30].
638 However, we modified the method to address differences in the samples used. Before
639 estimation of fate probabilities, we removed genes associated with the cell cycle
640 to ensure that we could specifically focus on genes that are not directly associated
641 with the cell cycle. For this, we collected cell-cycle genes[63] and filtered them. This led to
642 the removal of 38 genes from the 502 genes that were used to train temporal-

noSpliceVelo. We could then use the fate probabilities along with the gene expression profiles of each cell for further analysis, which can be found in our code repository https://github.com/BROOKELAB.

REFERENCES

1. Galani, I.E., Triantafyllia, V., Eleminiadou, E.-E., Koltsida, O., Stavropoulos, A., Manioudaki, M., Thanos, D., Doyle, S.E., Kotenko, S.V., Thanopoulou, K., et al. (2017). Interferon-λ Mediates Non-redundant Front-Line Antiviral Protection against Influenza Virus Infection without Compromising Host Fitness. Immunity *46*, 875-890.e6. https://doi.org/10.1016/j.immuni.2017.04.025.

2. Sheehan, K.C.F., Lazear, H.M., Diamond, M.S., and Schreiber, R.D. (2015). Selective Blockade of Interferon-α and -β Reveals Their Non-Redundant Functions in a Mouse Model of West Nile Virus Infection. PLOS ONE *10*, e0128636. https://doi.org/10.1371/journal.pone.0128636.

3. Piperakis, A., Galani, I.E., and Andreakos, E. (2024). Type III interferons in innate and adaptive immunity in the respiratory tract. Curr. Opin. Immunol. *87*, 102430. https://doi.org/10.1016/j.coi.2024.102430.

4. Boehmer, D., and Zanoni, I. (2025). Interferons in health and disease. Cell *188*, 4480–4504. https://doi.org/10.1016/j.cell.2025.06.044.

5. Duncan, C.J.A., Randall, R.E., and Hambleton, S. (2021). Genetic Lesions of Type I Interferon Signalling in Human Antiviral Immunity. Trends Genet. *37*, 46–58. https://doi.org/10.1016/J.TIG.2020.08.017.

6. Lazear, H.M., Schoggins, J.W., and Diamond, M.S. (2019). Shared and Distinct Functions of Type I and Type III Interferons. Immunity *50*, 907–923. https://doi.org/10.1016/j.immuni.2019.03.025.

7. Kato, H., Takeuchi, O., Mikamo-Satoh, E., Hirai, R., Kawai, T., Matsushita, K., Hiiragi, A., Dermody, T.S., Fujita, T., and Akira, S. (2008). Length-dependent recognition of double-stranded ribonucleic acids by retinoic acid–inducible gene-I and melanoma differentiation–associated gene 5. J. Exp. Med. *205*, 1601–1610. https://doi.org/10.1084/jem.20080091.

8. Rehwinkel, J., and Gack, M.U. (2020). RIG-I-like receptors: their regulation and roles in RNA sensing. Nat. Rev. Immunol. *20*, 537–551. https://doi.org/10.1038/s41577-020-0288-3.

9. Kato, H., Takeuchi, O., Sato, S., Yoneyama, M., Yamamoto, M., Matsui, K., Uematsu, S., Jung, A., Kawai, T., Ishii, K.J., et al. (2006). Differential roles of MDA5 and RIG-I helicases in the recognition of RNA viruses. Nature *441*, 101–105. https://doi.org/10.1038/nature04734.

680 10. Sun, J., Vera, J.C., Drnevich, J., Lin, Y.T., Ke, R., and Brooke, C.B. (2020). Single
681 cell heterogeneity in influenza A virus gene expression shapes the innate antiviral
682 response to infection. PLOS Pathog. *16*, e1008671.
683 https://doi.org/10.1371/journal.ppat.1008671.

684 11. Russell, A.B., Trapnell, C., and Bloom, J.D. (2018). Extreme heterogeneity of
685 influenza virus infection in single cells. eLife *7*. https://doi.org/10.7554/eLife.32303.

686 12. Ramos, I., Smith, G., Ruf-Zamojski, F., Martinez-Romero, C., Fribourg, M., Carbajal,
687 E.A., Hartmann, B.M., Nair, V.D., Marjanovic, N., Monteagudo, P.L., et al. (2019).
688 Innate immune response to influenza virus at single-cell resolution in human
689 epithelial cells revealed paracrine induction of interferon lambda 1. J. Virol.
690 https://doi.org/10.1128/JVI.00559-19.

691 13. Drayman, N., Patel, P., Vistain, L., and Tay, S. (2019). HSV-1 single-cell analysis
692 reveals the activation of anti-viral and developmental programs in distinct sub-
693 populations. eLife *8*, e46339. https://doi.org/10.7554/eLife.46339.

694 14. Bruurs, L.J.M., Müller, M., Schipper, J.G., Rabouw, H.H., Boersma, S., Van
695 Kuppeveld, F.J.M., and Tanenbaum, M.E. (2023). Antiviral responses are shaped by
696 heterogeneity in viral replication dynamics. Nat. Microbiol. *8*, 2115–2129.
697 https://doi.org/10.1038/s41564-023-01501-z.

698 15. Bhushal, S., Wolfsmüller, M., Selvakumar, T.A., Kemper, L., Wirth, D., Hornef, M.W.,
699 Hauser, H., and Köster, M. (2017). Cell Polarization and Epigenetic Status Shape
700 the Heterogeneous Response to Type III Interferons in Intestinal Epithelial Cells.
701 Front. Immunol. *8*, 671. https://doi.org/10.3389/fimmu.2017.00671.

702 16. Wyler, E., Franke, V., Menegatti, J., Kocks, C., Boltengagen, A., Praktiknjo, S.,
703 Walch-Rückheim, B., Bosse, J., Rajewsky, N., Grässer, F., et al. (2019). Single-cell
704 RNA-sequencing of herpes simplex virus 1-infected cells connects NRF2 activation
705 to an antiviral program. Nat. Commun. *10*, 4878. https://doi.org/10.1038/s41467-
706 019-12894-z.

707 17. Preedy, M.K., White, M.R.H., and Tergaonkar, V. (2024). Cellular heterogeneity in
708 TNF/TNFR1 signalling: live cell imaging of cell fate decisions in single cells. Cell
709 Death Dis. *15*, 1–12. https://doi.org/10.1038/s41419-024-06559-z.

710 18. Goyal, Y., Busch, G.T., Pillai, M., Li, J., Boe, R.H., Grody, E.I., Chelvanambi, M.,
711 Dardani, I.P., Emert, B., Bodkin, N., et al. (2023). Diverse clonal fates emerge upon
712 drug treatment of homogeneous cancer cells. Nat. 2023 6207974 *620*, 651–659.
713 https://doi.org/10.1038/s41586-023-06342-8.

714 19. Carter, B., and Zhao, K. (2020). The epigenetic basis of cellular heterogeneity. Nat.
715 Rev. Genet. 2020 224 *22*, 235–250. https://doi.org/10.1038/s41576-020-00300-0.

716 20. Yang, J., Tian, B., Sun, H., Garofalo, R.P., and Brasier, A.R. (2017). Epigenetic
717 silencing of IRF1 dysregulates type III interferon responses to respiratory virus

718 infection in epithelial to mesenchymal transition. Nat. Microbiol. 2017 28 *2*, 1–11.
719 https://doi.org/10.1038/nmicrobiol.2017.86.

720 21. Reffsin, S., Miller, J., Ayyanathan, K., Dunagin, M.C., Heyman, Y., Jain, N., Schultz,
721 D.C., Cherry, S., and Raj, A. (2025). Single-cell susceptibility to viral infection is
722 driven by variable cell states. Cell. https://doi.org/10.1016/j.cell.2025.10.021.

723 22. Rivera-Cardona, J., Mahajan, T., Kakuturu, N.R., Teo, Q.W., Lederer, J., Thayer,
724 E.A., Rowland, E.F., Heimburger, K., Sun, J., McDonald, C.A., et al. (2025). Intrinsic
725 OASL expression licenses interferon induction during influenza A virus infection.
726 Preprint, https://doi.org/10.1101/2025.03.14.643375.

727 23. Russell, A.B., Elshina, E., Kowalsky, J.R., Te Velthuis, A.J.W., and Bloom, J.D.
728 (2019). Single-cell virus sequencing of influenza infections that trigger innate
729 immunity. J. Virol. https://doi.org/10.1128/JVI.00500-19.

730 24. Killip, M.J., Jackson, D., Pérez-Cidoncha, M., Fodor, E., and Randall, R.E. (2017).
731 Single-cell studies of IFN-β promoter activation by wild-type and NS1-defective
732 influenza A viruses. J. Gen. Virol. *98*, 357–363. https://doi.org/10.1099/jgv.0.000687.

733 25. Zhao, M., Zhang, J., Phatnani, H., Scheu, S., and Maniatis, T. (2012). Stochastic
734 Expression of the Interferon-β Gene. PLoS Biol. *10*, e1001249.
735 https://doi.org/10.1371/journal.pbio.1001249.

736 26. Schulte, M.B., and Andino, R. (2014). Single-cell analysis uncovers extensive
737 biological noise in poliovirus replication. J. Virol. *88*, 6205–6212.
738 https://doi.org/10.1128/JVI.03539-13.

739 27. Guo, F., Li, S., Caglar, M.U., Mao, Z., Liu, W., Woodman, A., Arnold, J.J., Wilke,
740 C.O., Huang, T.J., and Cameron, C.E. (2017). Single-Cell Virology: On-Chip
741 Investigation of Viral Infection Dynamics. Cell Rep. *21*, 1692–1704.
742 https://doi.org/10.1016/j.celrep.2017.10.051.

743 28. Kramer, E.E., Steadman, P.E., Epp, J.R., Frankland, P.W., and Josselyn, S.A.
744 (2018). Assessing Individual Neuronal Activity Across the Intact Brain: Using
745 Hybridization Chain Reaction (HCR) to Detect *Arc* mRNA Localized to the Nucleus
746 in Volumes of Cleared Brain Tissue: Kramer et al. Curr. Protoc. Neurosci. *84*, e49.
747 https://doi.org/10.1002/cpns.49.

748 29. Rivera-Cardona, J., Kakuturu, N., Rowland, E.F., Teo, Q.W., Thayer, E.A., Tan,
749 T.J.C., Sun, J., Kieffer, C., Wu, N.C., and Brooke, C.B. (2024). Seasonal influenza a
750 virus lineages exhibit divergent abilities to antagonize interferon induction and
751 signaling. PLOS Pathog. *20*, e1012727.
752 https://doi.org/10.1371/journal.ppat.1012727.

753 30. Mahajan, T., and Maslov, S. (2024). noSpliceVelo infers gene expression dynamics
754 without separating unspliced and spliced transcripts. Preprint,
755 https://doi.org/10.1101/2024.08.08.607261.

31. Pucella, J.N., Maqueda-Alfaro, R.A., Ni, H., Bandeira Sulczewski, F., Eichinger, A., Esteva, E., Ra, A.C., Das, A., Perez, O.A., Feng, J., et al. (2025). Tonic type I interferon signaling optimizes the antiviral function of plasmacytoid dendritic cells. Nat. Immunol. https://doi.org/10.1038/s41590-025-02279-4.

32. Gewaid, H., and Bowie, A.G. (2024). Regulation of type I and type III interferon induction in response to pathogen sensing. Curr. Opin. Immunol. *87*, 102424. https://doi.org/10.1016/j.coi.2024.102424.

33. Szklarczyk, D., Kirsch, R., Koutrouli, M., Nastou, K., Mehryary, F., Hachilif, R., Gable, A.L., Fang, T., Doncheva, N.T., Pyysalo, S., et al. (2023). The STRING database in 2023: protein–protein association networks and functional enrichment analyses for any sequenced genome of interest. Nucleic Acids Res. *51*, D638–D646. https://doi.org/10.1093/nar/gkac1000.

34. Schoggins, J.W. (2019). Interferon-Stimulated Genes: What Do They All Do? Annu. Rev. Virol. *6*, 567–584. https://doi.org/10.1146/annurev-virology-092818-015756.

35. Yang, H., Winkler, W., and Wu, X. (2021). Interferon Inducer IFI35 Regulates RIG-I-Mediated Innate Antiviral Response through Mutual Antagonism with Influenza Virus Protein NS1. J. Virol. *95*, 10.1128/jvi.00283-21. https://doi.org/10.1128/jvi.00283-21.

36. Vicenzi, E., and Poli, G. (2018). The interferon-stimulated gene *TRIM22*: A double-edged sword in HIV-1 infection. Cytokine Growth Factor Rev. *40*, 40–47. https://doi.org/10.1016/j.cytogfr.2018.02.001.

37. Maniatis, T., Falvo, J.V., Kim, T.H., Kim, T.K., Lin, C.H., Parekh, B.S., and Wathelet, M.G. (1998). Structure and Function of the Interferon- Enhanceosome. Cold Spring Harb. Symp. Quant. Biol. *63*, 609–620. https://doi.org/10.1101/sqb.1998.63.609.

38. Thanos, D., and Maniatis, T. (1995). Virus induction of human IFNβ gene expression requires the assembly of an enhanceosome. Cell *83*, 1091–1100. https://doi.org/10.1016/0092-8674(95)90136-1.

39. Karin, M. (1995). The Regulation of AP-1 Activity by Mitogen-activated Protein Kinases. J. Biol. Chem. *270*, 16483–16486. https://doi.org/10.1074/jbc.270.28.16483.

40. Aggarwal, B.B., Gupta, S.C., and Kim, J.H. (2012). Historical perspectives on tumor necrosis factor and its superfamily: 25 years later, a golden journey. Blood *119*, 651–665. https://doi.org/10.1182/blood-2011-04-325225.

41. Westwick, J.K., Weitzel, C., Minden, A., Karin, M., and Brenner, D.A. (1994). Tumor necrosis factor alpha stimulates AP-1 activity through prolonged activation of the c-Jun kinase. J. Biol. Chem. *269*, 26396–26401. https://doi.org/10.1016/S0021-9258(18)47207-9.

42. Brenner, D.A., O'Hara, M., Angel, P., Chojkier, M., and Karin, M. (1989). Prolonged activation of jun and collagenase genes by tumour necrosis factor-α. Nature *337*, 661–663. https://doi.org/10.1038/337661a0.

43. Ostojic, A., Vrhovac, R., and Verstovsek, S. (2011). Ruxolitinib: a new JAK1/2 inhibitor that offers promising options for treatment of myelofibrosis. Future Oncol. Lond. Engl. *7*, 1035–1043. https://doi.org/10.2217/fon.11.81.

44. Yarilina, A., Park-Min, K.H., Antoniv, T., Hu, X., and Ivashkiv, L.B. (2008). TNF activates an IRF1-dependent autocrine loop leading to sustained expression of chemokines and STAT1-dependent type I interferon–response genes. Nat. Immunol. 2008 94 *9*, 378–387. https://doi.org/10.1038/ni1576.

45. Zhang, T., Inesta-Vaquera, F., Niepel, M., Zhang, J., Ficarro, S.B., MacHleidt, T., Xie, T., Marto, J.A., Kim, N., Sim, T., et al. (2012). Discovery of Potent and Selective Covalent Inhibitors of JNK. Chem. Biol. *19*, 140–154. https://doi.org/10.1016/J.CHEMBIOL.2011.11.010.

46. Favata, M.F., Horiuchi, K.Y., Manos, E.J., Daulerio, A.J., Stradley, D.A., Feeser, W.S., Van Dyk, D.E., Pitts, W.J., Earl, R.A., Hobbs, F., et al. (1998). Identification of a Novel Inhibitor of Mitogen-activated Protein Kinase Kinase*. J. Biol. Chem. *273*, 18623–18632. https://doi.org/10.1074/jbc.273.29.18623.

47. Zhang, T., Inesta-Vaquera, F., Niepel, M., Zhang, J., Ficarro, S.B., Machleidt, T., Xie, T., Marto, J.A., Kim, N., Sim, T., et al. (2012). Discovery of potent and selective covalent inhibitors of JNK. Chem. Biol. *19*, 140–154. https://doi.org/10.1016/j.chembiol.2011.11.010.

48. Peterson, A.F., Ingram, K., Huang, E.J., Parksong, J., McKenney, C., Bever, G.S., and Regot, S. (2022). Systematic analysis of the MAPK signaling network reveals MAP3K-driven control of cell fate. Cell Syst. *13*, 885-894.e4. https://doi.org/10.1016/j.cels.2022.10.003.

49. Wu, C.C.-C., Peterson, A., Zinshteyn, B., Regot, S., and Green, R. (2020). Ribosome Collisions Trigger General Stress Responses to Regulate Cell Fate. Cell *182*, 404-416.e14. https://doi.org/10.1016/j.cell.2020.06.006.

50. Arthur, J.S.C., and Ley, S.C. (2013). Mitogen-activated protein kinases in innate immunity. Nat. Rev. Immunol. *13*, 679–692. https://doi.org/10.1038/nri3495.

51. Wang, W., Xu, L., Brandsma, J.H., Wang, Y., Hakim, M.S., Zhou, X., Yin, Y., Fuhler, G.M., van der Laan, L.J.W., van der Woude, C.J., et al. (2016). Convergent Transcription of Interferon-stimulated Genes by TNF-α and IFN-α Augments Antiviral Activity against HCV and HEV. Sci. Rep. *6*, 25482. https://doi.org/10.1038/srep25482.

52. Veckman, V., Österlund, P., Fagerlund, R., Melén, K., Matikainen, S., and Julkunen, I. (2006). TNF-α and IFN-α enhance influenza-A-virus-induced chemokine gene

830 expression in human A549 lung epithelial cells. Virology *345*, 96–104.
831 https://doi.org/10.1016/j.virol.2005.09.043.

832 53. Tliba, O., Tliba, S., Da Huang, C., Hoffman, R.K., DeLong, P., Panettieri, R.A., and
833 Amrani, Y. (2003). Tumor Necrosis Factor α Modulates Airway Smooth Muscle
834 Function via the Autocrine Action of Interferon β*. J. Biol. Chem. *278*, 50615–50623.
835 https://doi.org/10.1074/jbc.M303680200.

836 54. Yamane, D., Feng, H., Rivera-Serrano, E.E., Selitsky, S.R., Hirai-Yuki, A., Das, A.,
837 McKnight, K.L., Misumi, I., Hensley, L., Lovell, W., et al. (2019). Basal expression of
838 interferon regulatory factor 1 drives intrinsic hepatocyte resistance to multiple RNA
839 viruses. Nat. Microbiol. 2019 47 *4*, 1096–1104. https://doi.org/10.1038/s41564-019-
840 0425-6.

841 55. Blanpain, C., Horsley, V., and Fuchs, E. (2007). Epithelial Stem Cells: Turning over
842 New Leaves. Cell *128*, 445–458. https://doi.org/10.1016/j.cell.2007.01.014.

843 56. Daman, A.W., and Josefowicz, S.Z. (2021). Epigenetic and transcriptional control of
844 interferon-β. J. Exp. Med. *218*, e20210039. https://doi.org/10.1084/jem.20210039.

845 57. Gao, Z., Li, W., Mao, X., Huang, T., Wang, H., Li, Y., Liu, B., Zhong, J., Renjie, C.,
846 Jin, J., et al. (2021). Single-nucleotide methylation specifically represses type I
847 interferon in antiviral innate immunity. J. Exp. Med. *218*, e20201798.
848 https://doi.org/10.1084/jem.20201798.

849 58. Kamada, R., Yang, W., Zhang, Y., Patel, M.C., Yang, Y., Ouda, R., Dey, A.,
850 Wakabayashi, Y., Sakaguchi, K., Fujita, T., et al. (2018). Interferon stimulation
851 creates chromatin marks and establishes transcriptional memory. Proc. Natl. Acad.
852 Sci. *115*, E9162–E9171. https://doi.org/10.1073/pnas.1720930115.

853 59. Manivasagam, S., Han, J., Teghanemt, A., Keen, H., Sownthirarajan, B., Cheng, B.,
854 Singh, A., Lewis, A., Vogel, O.A., Loganathan, G., et al. (2025). Transcriptional
855 repressor Capicua is a gatekeeper of cell-intrinsic interferon responses. Cell Host
856 Microbe *33*, 512-528.e7. https://doi.org/10.1016/j.chom.2025.02.017.

857 60. Panda, A., Suvakov, M., Mariani, J., Drucker, K.L., Park, Y., Jang, Y., Kollmeyer,
858 T.M., Sarkar, G., Bae, T., Kim, J.J., et al. (2023). Clonally Selected Lines After
859 CRISPR-Cas Editing Are Not Isogenic. CRISPR J. *6*, 176–182.
860 https://doi.org/10.1089/crispr.2022.0050.

861 61. Bradley, H., Barr, J.N., and Stacey, M. (2024). Single cell variation and rapid
862 emergence of phenotypic heterogeneity in cell lines- a cautionary tale for devotees
863 of CRISPR-Cas9. Preprint at bioRxiv, https://doi.org/10.1101/2024.09.27.615490.

864 62. Callard, R., George, A.J.T., and Stark, J. (1999). Cytokines, Chaos, and Complexity.
865 Immunity *11*, 507–513. https://doi.org/10.1016/S1074-7613(00)80125-9.

866 63. Viner-Breuer, R., Yilmaz, A., Benvenisty, N., and Goldberg, M. (2019). The
867 essentiality landscape of cell cycle related genes in human pluripotent and cancer
868 cells. Cell Div. *14*, 15. https://doi.org/10.1186/s13008-019-0058-4.

869

870

871